Constitutive Modelling of Biaxially Stressed Wood for the Analysis of Layered Wooden Shells

Herbert W. Müllner [1], Peter Mackenzie-Helnwein [2] and Josef Eberhardsteiner [1]

[1] *Institute for Strength of Materials, Vienna University of Technology, Vienna, Austria*
[2] *Department of Civil and Environmental Engineering, University of Washington, Seattle, United States*

Abstract
In this contribution a brief overview of the development of an orthotropic material model for the simulation of clear spruce wood under simultaneous biaxial in-plane stresses and transverse shear stresses is given. The model considers an initially linear elastic domain as well as hardening and softening behaviour at higher states of stress and strain, respectively. Combining the advantage of a smooth single-surface plasticity model with the identification of several modes of failure is the key to the novel mathematical formulation. The applicability of the new constitutive model will be demonstrated by means of a nonlinear finite element analysis of a layered cylindrical shell.

1. INTRODUCTION

Realistic finite element ultimate load analysis of layered wooden shells requires knowledge of both, suitable constitutive equations for the prediction of the deformation behaviour of biaxially loaded solid wood and the transverse shear forces inducing shear stresses in cross-sections perpendicular to the middle surface of the shell. Thus, a fully three-dimensional constitutive model is needed.

The model development is based on a comprehensive test series on clear spruce wood by EBERHARDSTEINER [2]. The respective biaxial experiments provide the necessary information concerning the stress-strain relations in the pre-failure domain as well as the failure locations for arbitrary strain paths. The obtained failure locations reveal an elliptic shape of the failure envelope. In [2] that envelope is decribed by means of the orthotropic failure criterion by TSAI & WU [8] which identifies failure states as a boundary of a linear elastic domain.

By defining characteristic strength values, depending on the material parameters of the elliptic failure criterion, MÜLLNER [6] combined these values with micromechanically motivated failure modes identified by MACKENZIE-HELNWEIN et al. [4]. The determination of the material parameters results in a system of nonlinear equations. Thus, the advantage of a single-surface model has to be paid for by the extra effort of locally solving these nonlinear equations. The application of the classical return mapping algorithm by SIMO & HUGHES [7] yields an unsymmetric consistent tangent for this material model.

This contribution reviews ideas first introduced with a multi-surface approach [4] in the attempt to apply them to the initial single-surface description suggested by [2]. A related study was successfully performed by [6] for the in-plane biaxial loading. The generalization of this formulation for stress states observed in layered shells was done by MACKENZIE-HELNWEIN et al. [5].

In Chapter 2 four failure modes of biaxial stressed wood are identified. Chapter 3 refers to the material model, where in Section 3.1 the used yield surface is described. Because of the brittle tensile and the ductile compressive behaviour of wood the formulation of different evolution laws by means of strain-like primary variables is required. Therefore a compatibility condition for the material parameters is needed (Section 3.2). For the material model an associated flow rule (Section 3.3) and a non-associated hardening and softening rule (Section 3.4) is used. Chapter 4 gives an example for the visualisation of the yield surface before and after plastic deformations. Finally, a representative example analysis is given in Chapter 5.

2. FUNDAMENTAL FAILURE MECHANISMS FOR BIAXIALLY STRESSED WOOD

Based on a cruciform specimen made out of clear spruce wood without imperfections such as knots and a moisture content of 12 %, a series of 439 displacement-driven biaxial strength tests were performed [2]. These tests cover the whole set of distinguishable stress states for an orthotropic material under plane stress conditions. The individual tests differ in two mechanical parameters:

- *Grain angle* φ – it is the angle between principal loading direction and the grain direction L.
- *Displacement ratio* κ – it is defined as $\kappa \approx \varepsilon_{11} : \varepsilon_{22}$, with ε_{11} and ε_{22} according to Fig. 1.

The obtained failure locations reveal an elliptic shape of the failure envelope by TSAI & WU [8]. This failure criterion corresponds with a second-order tensor polynomial and is shown in Fig. 1.

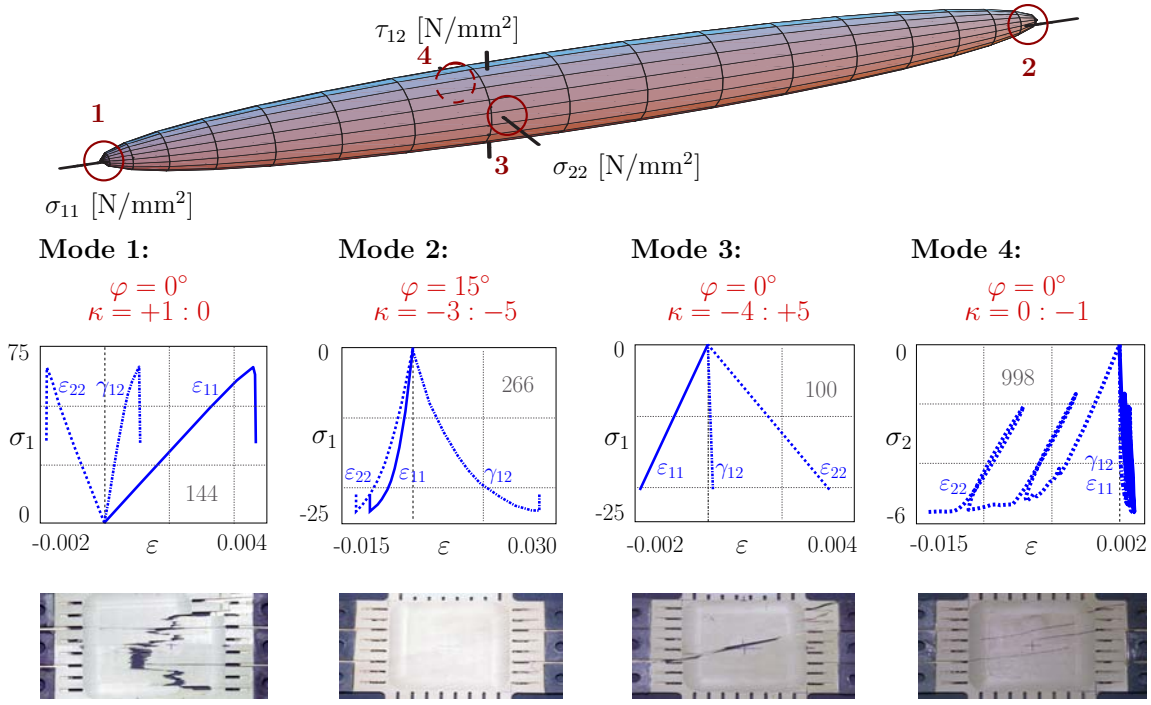

Figure 1 - Elliptic failure envelope by Tsai & Wu and characteristic stress-strain curves and fracture types for characteristic biaxial loading situations

Analyzing the stress-strain relations for different load ratios MACKENZIE-HELNWEIN et al. [4] characterised four modes of failure, illustrated in Fig. 1 by a stress-strain diagram and an image of the specimen at fracture:

- Mode 1 – brittle tensile failure in fibre direction,
- Mode 2 – compressive failure in fibre direction,
- Mode 3 – brittle tensile failure perpendicular to grain, and
- Mode 4 – ductile compressive behaviour perpendicular to grain.

At large deformations, both compressive modes 2 and 4, show a phenomenon called *densification* which causes an equilibrium state of internal stresses in the cell structure [1]. Building up these internal stresses does not cause additional dissipation though the effective compressive strength increases.

Concerning stress states in layered wooden shells, a fifth failure mode may become relevant. It is controlled by transverse shear stresses and thus cannot be observed in the existing biaxial tests by EBERHARDSTEINER [2]. Nevertheless, that failure mechanism is closely related to shear failure in a plane perpendicular to the radial direction [5].

Typically, single-surface models do not permit the identification of these micromechanical failure modes. Adopt an associated hardening, the single-surface model would admit only one hardening-parameter. Thus, the form of the yield surface would change equally in all directions. Therefore, the formulation of a non-associated hardening or softening rule has to occur, as shown in the next chapter.

3. SINGLE-SURFACE PLASTICITY MODEL

3.1. Orthotropic yield surface

The orientation of wood is characterized by its growth direction in the stem, i.e., the longitudinal or fibre direction *L*, the radial direction *R*, and the tangential direction *T*.

The concept of a single-surface model offers a reasonably simple mathematical description of an orthotropic yield surface by means of six independent material parameters for plane stress states in the *LR*-plane and seven ones for including the effect of transverse shear. The basis of the single-surface description is the elliptic yield condition by TSAI & WU [8]

$$\begin{aligned} f(\boldsymbol{\sigma},\mathbf{p}^*) = {} & a_{LL}\,\sigma_L + a_{RR}\,\sigma_R + b_{LLLL}\,\sigma_L^{\,2} + b_{RRRR}\,\sigma_R^{\,2} + \\ & + 2\,b_{LLRR}\sigma_L\sigma_R + 4\,b_{LRLR}\tau_{LR}^{\,2} + 4\,b_{RTRT}\tau_{RT}^{\,2} + 4\,b_{TLTL}\tau_{TL}^{\,2} - 1 = 0 \end{aligned} \tag{1}$$

where the seven independent material parameters a_{ij} and b_{ijkl} $(i,j,k,l \in \{L,R\})$ are listed in

$$\mathbf{p}^* = \begin{Bmatrix} a_{LL} \\ a_{RR} \\ b_{LLLL} \\ b_{RRRR} \\ b_{LLRR} \\ b_{LRLR} \\ b_{RTRT} \end{Bmatrix} = \begin{Bmatrix} -0.004725\ \mathrm{mm^2/N} \\ -0.030672\ \mathrm{mm^2/N} \\ +0.000309\ \mathrm{mm^4/N^2} \\ +0.054853\ \mathrm{mm^4/N^2} \\ +0.000382\ \mathrm{mm^4/N^2} \\ +0.003452\ \mathrm{mm^4/N^2} \\ +0.003452\ \mathrm{mm^4/N^2} \end{Bmatrix} . \tag{2}$$

By introducing the effective shear stresses

$$\tau_R = \sqrt{\tau_{LR}^{\,2} + \tau_{RT}^{\,2}} \qquad \text{and} \qquad \tau_T = \sqrt{\tau_{RT}^{\,2} + \tau_{TL}^{\,2}} \tag{3}$$

and associating it with shear failure in planes perpendicular to the *R*- and *T*-direction, the material parameter b_{TLTL} in (1) can be equated with b_{RTRT}. The determined yield surface is shown in Fig. 2.

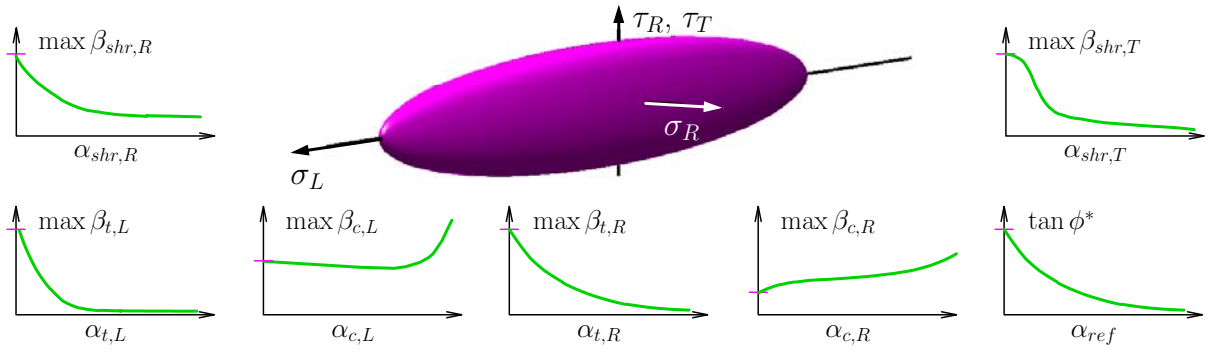

Figure 2 - Yield surface of single-surface material model in the orthotropic stress space and evolution laws for the strength values depending on the strain-like primary variables α_i

In order to consider the different failure mechanisms mentioned in Chapter 2 it is necessary to formulate a non-associated hardening and softening rule. Because of the seven independent material parameters in (2) the hardening and softening rule consists of seven entries, too. These evolutions laws, depicted in Fig. 2, are collected in the vector $\mathbf{R}_p$ of (5). They describe the strength properties of the different failure modes by means of strain-like primary variables α_i ($i \in \{(t,L), (c,L), (t,R), (c,R), (ref), (shr,R), (shr,T)\}$.

The strength values used in the evolution laws are the six maxima of the strength values, $max\ \beta_{i,j}$ ($i \in \{t,c\}, j \in \{L,R\}$) as well as $\beta_{shr,R}$ and $\beta_{shr,T}$, and the inclination $tan\ \phi^*$ of the yield surface in the plane $\tau_R = 0$ (see Figs. 3(a) and 3(b)). In order to connect the seven strength values with the corresponding failure modes, it is necessary to formulate a compatibility condition as shown in the next section.

3.2. Compatibility condition for the material parameters

In Figs. 3(a) and 3(b) the considered strength values are defined by means of the chosen elliptical yield surface. If plastic strains occur the yield surface will change in size and shape as shown in the figures.

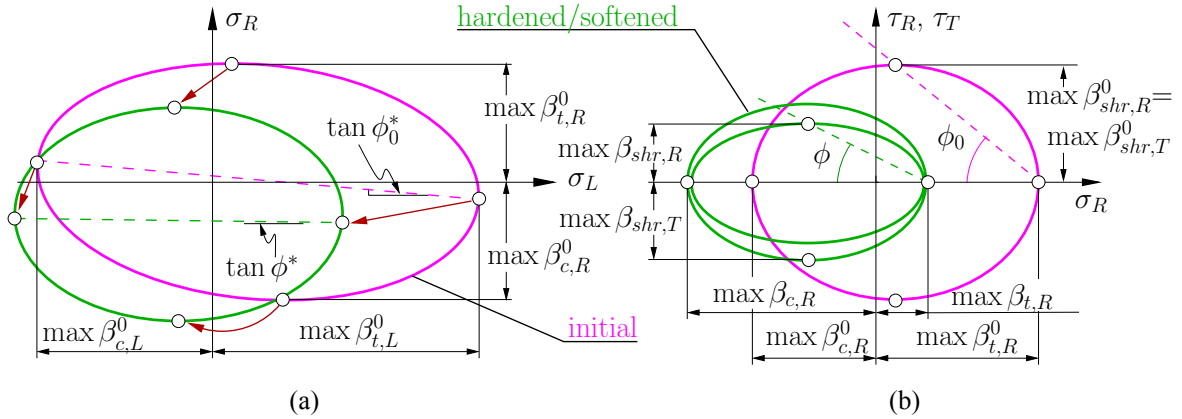

Figure 3 - Characteristic strength values of the single-surface model
(a) tensile and compressive strength in the plane $\tau_{LR} = 0$, (b) shear strength in the plane $\sigma_L = 0$

The seven strength values are on the one hand controlled by the vector **p*** and on the other hand multiplied by the evolution laws. With these two definitions a residual vector

$$\mathbf{R} = \mathbf{R}_\beta - \mathbf{R}_p = \begin{Bmatrix} \max \beta_{t,L}(\mathbf{p}^*) \\ \max \beta_{c,L}(\mathbf{p}^*) \\ \max \beta_{t,R}(\mathbf{p}^*) \\ \max \beta_{c,R}(\mathbf{p}^*) \\ \tan \phi^*(\mathbf{p}^*) \\ \max \beta_{shr,R}(\mathbf{p}^*) \\ \max \beta_{shr,T}(\mathbf{p}^*) \end{Bmatrix} - \begin{Bmatrix} \max \beta_{t,L}(\alpha_{t,L}) \\ \max \beta_{c,L}(\alpha_{c,L}) \\ \max \beta_{t,R}(\alpha_{t,R}) \\ \max \beta_{c,R}(\alpha_{c,R}) \\ \tan \phi^*(\alpha_{ref}) \\ \max \beta_{shr,R}(\alpha_{c,L}, \alpha_{c,R}, \alpha_{shr,R}) \\ \max \beta_{shr,T}(\alpha_{shr,T}) \end{Bmatrix} = \mathbf{0} \tag{4}$$

can be defined, where

$$\mathbf{R}_p = \begin{Bmatrix} \max \beta^0_{t,L}\, e^{-k_{t,L}\,\alpha_{t,L}} \\ \max \beta^0_{c,L} - Y_{1,L}\,(1 - e^{-k_{c,L}\,\alpha_{c,L}}) + q_L(\alpha_{c,L}) \\ \max \beta^0_{t,R}\, e^{-k_{t,R}\,\alpha_{t,R}} \\ \max \beta^0_{c,R} + Y_{1,R}\,(1 - e^{-k_{c,R}\,\alpha_{c,R}}) + q_R(\alpha_{c,R}) \\ \tan \phi^*_0\, e^{-k_{t,R}\,\alpha_{ref}} \\ \dfrac{\max \beta_{t,R}\,(\alpha_{t,R}) + \max \beta_{c,R}\,(\alpha_{c,R})}{2} \tan[\phi_\infty + (\phi_0 - \phi_\infty)\, e^{-k_{shr,R}\,\alpha_{shr,R}}] \\ \max \beta^0_{shr,T}\, e^{-k_{shr,T}\,\alpha_{shr,T}^2} \end{Bmatrix} \tag{5}$$

is the stress vector function. If plastic strains occur, the residual vector **R** is not satisfied and the components of the vector **p*** have to be modified. The obtained nonlinear equation system is solved by means of the NEWTON-RAPHSON-method. The new entries of **p*** define a new yield surface without changing the mathematical form of (1).

The increasing of the compressive strength due to *densification* is modelled by means of the terms

$$q_L(\alpha_{c,L}) = H_{L,d}\,\frac{\langle \alpha_{c,L} - \alpha_{L,d} \rangle^2}{\alpha_{L,\infty} - \alpha_{c,L}} \qquad \text{and} \qquad q_R(\alpha_{c,R}) = H_{L,R}\,\frac{\langle \alpha_{c,R} - \alpha_{R,d} \rangle^2}{\alpha_{R,\infty} - \alpha_{c,R}}\ , \tag{6}$$

where $H_{K,d}$ is a hardening stiffness parameter, $\alpha_{K,d}$ and $\alpha_{K,\infty}$ mark the onset of densification and the ultimate densification strain, respectively, ($K \in \{L,R\}$) and $\langle x \rangle = (x + |x|)/2$.

3.3. Associated flow rule – evolution law for plastic strains

The evolution law for the plastic strains can be described by means of a flow potential formulation by SIMO & HUGHES [5]. Under consideration of *associated plasticity* the flow rule reduces to

$$\dot{\boldsymbol{\varepsilon}}^{p} = \begin{Bmatrix} \varepsilon_L{}^{p} \\ \varepsilon_R{}^{p} \\ \gamma_{LR}{}^{p} \\ \gamma_{RT}{}^{p} \\ \gamma_{TL}{}^{p} \end{Bmatrix} = \dot{\gamma}\frac{\partial f}{\partial \boldsymbol{\sigma}} = \dot{\gamma}\,\mathbf{r} = \dot{\gamma}\begin{Bmatrix} r_1 \\ r_2 \\ r_3 \\ r_4 \\ r_5 \end{Bmatrix} = \dot{\gamma}\begin{Bmatrix} a_{LL} + 2b_{LLLL}\,\sigma_L + 2b_{LLRR}\,\sigma_R \\ a_{RR} + 2b_{LLRR}\,\sigma_L + 2b_{RRRR}\,\sigma_R \\ 8b_{LRLR}\,\tau_{LR}{}^{2} \\ 8b_{RTRT}\,\tau_{RT}{}^{2} \\ 8b_{TLTL}\,\tau_{TL}{}^{2} \end{Bmatrix}, \tag{7}$$

with $\dot{\gamma}$ as a proportionality factor, the so-called consistency parameter.

3.4. Non-associated hardening and softening rule – evolution law for primary variables

Different evolution laws implicate different hardening and softening rules, respectively. Thus, the non-associated hardening or softening rule for the single-surface model results as

$$\dot{\boldsymbol{\alpha}} = \begin{Bmatrix} \alpha_{t,L} \\ \alpha_{c,L} \\ \alpha_{t,R} \\ \alpha_{c,R} \\ \alpha_{ref} \\ \alpha_{shr,R} \\ \alpha_{shr,T} \end{Bmatrix} = \dot{\gamma}\,\mathbf{s} = \dot{\gamma}\begin{Bmatrix} \langle\, r_1 \rangle \\ \langle -r_1 \rangle \\ \langle\, r_2 \rangle \\ \langle -r_2 \rangle \\ \langle\, r_2 \rangle \\ 2|r_3| \\ 2\left(|r_4| + |r_5|\right) \end{Bmatrix}. \tag{8}$$

4. VISUALISATION OF THE YIELD SURFACE

Because of the orthotropic characteristics of wood and the restriction to plane stress states, the visualisation of the elliptical yield surface in the orthotropic stress space (σ_L, σ_R, τ_{LR}) is advantageous [6]. In the present case, transverse shear stresses are considered, too.

Thus, the visualisation of the yield surface has to be modified, as shown in Fig. 4. The visualisation of one stress state is split into two pictures. Figure 4(a) shows the yield surface for the apparent stress state in the σ_L-σ_R-τ_R-stress space, and Fig. 4(b) shows it in the σ_L-σ_R-τ_T-stress space (for the definition of the effective shear stresses τ_R and τ_T see (3)).

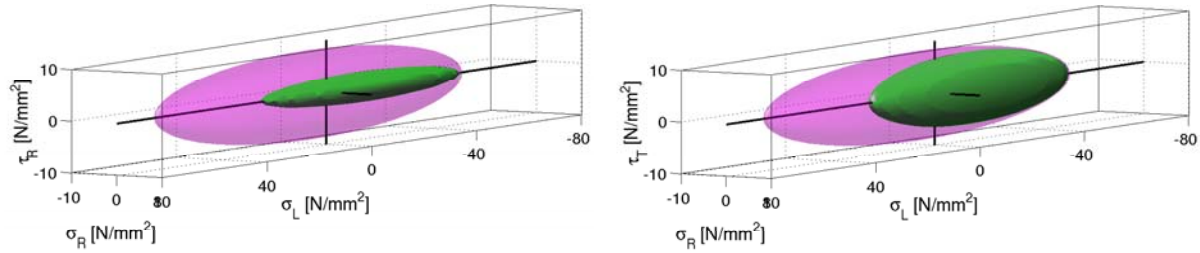

(a) (b)

Figure 4 - Initial (magenta) and modified (green) yield surfaces of single-surface material model: (a) in the σ_L-σ_R-τ_R-stress space (b) in the σ_L-σ_R-τ_T-stress space

Figure 4 shows as an example the initial and the modified yield surface in case of plastic deformations due to tensile loading in longitudinal direction. This kind of load is connected with a cascading crack pattern [4]. In the case of alternating loading the material accepts compressive loading despite of the crack.

5. NUMERICAL EXAMPLE

The suggested material model was used for the analysis of a cylindrical wooden shell with an opening and stiffening beams as shown in the horizontal projection of the shell in Fig. 5(a). The arch rise of the circular cylindrical shell is 2.00 m. With a length of 10.0 m and a width of 8.0 m, the thickness of the shell is only 48 mm. In thickness direction, the shell consists of three layers of equal thickness. The complete shell is made out of the same material but the grain angle varies for different layers. For instance, the outer layers have a grain angle of +30° with respect to the *xy* reference plane.

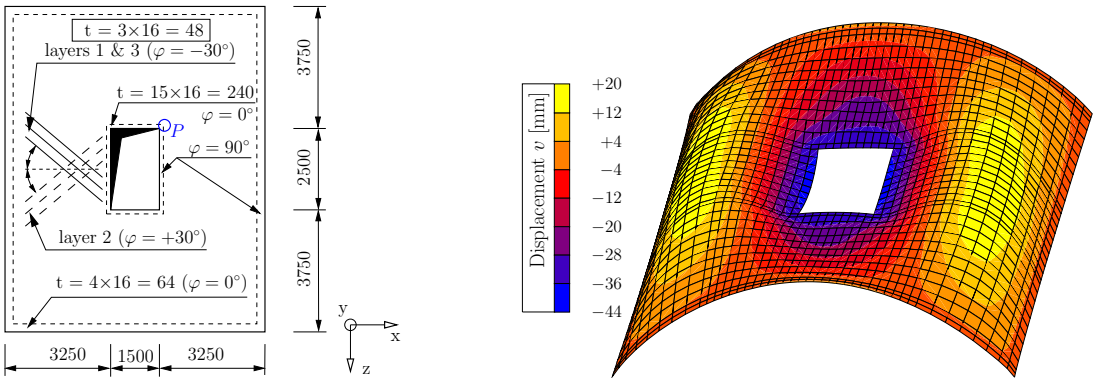

(a) (b)

Figure 5 - Cylindrical shell with opening
(a) shell geometry and orientation of boards, (b) vertical displacements at maximum applied load

Figure 5(b) shows the used finite element mesh. The minimum element size is 150 x 150 mm, the largest one is 300 x 300 mm. Moreover, the figure shows the deformed shape at a scaling factor of 15. The maximum displacements are along the longitudinal edges of the opening. The deformation pattern shows point symmetry about the centre of the structure which corresponds to the point symmetric composition of the shell. The material parameters from [5] and [6] are summarized in Table 1.

Table 1: Material parameters for the single-surface plasticity model

elastic behaviour	E_L =	13000 N/mm²	E_R =	700 N/mm²	ν_{LR} =	0.50
	G_{LR} =	632 N/mm²	G_{RT} =	222 N/mm²	G_{TL} =	470 N/mm²
behaviour in grain direction	$k_{t,L}$ =	118.18	$Y_{l,L}$ =	10.00 N/mm²	$\alpha_{L,d}$ =	0.50
	$k_{c,L}$ =	3.02	$H_{L,d}$ =	15.00 N/mm²	$\alpha_{L,\infty}$ =	0.75
behaviour in radial direction	$k_{t,R}$ =	45.60	$Y_{l,R}$ =	1.80 N/mm²	$\alpha_{R,d}$ =	0.10
	$k_{c,R}$ =	30.00	$H_{R,d}$ =	2.00 N/mm²	$\alpha_{R,\infty}$ =	0.75
shear in *LR*-plane	$k_{shr,R}$ =	86.00	ϕ_0 =	63.3°	ϕ_∞ =	35.0°
shear in *TL*-plane	$k_{shr,T}$ =	2091.17				

Two different load cases were considered in the analysis. First, a uniformly distributed dead load with a density of 0.45 g/cm³, second, a live load of up to 225 kN, equally distributed along the stiffening beam which surrounds the opening.

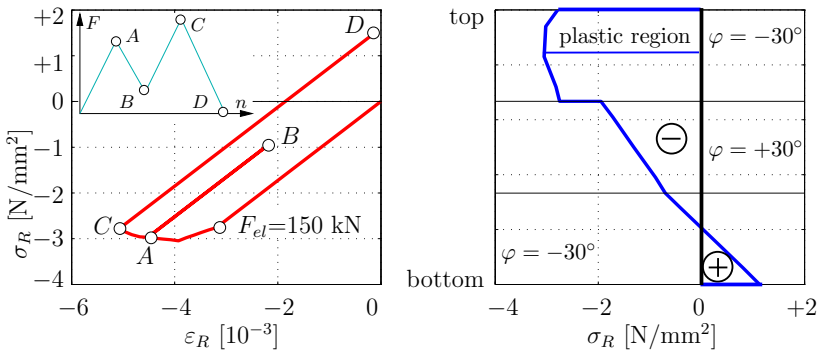

(a) (b)

Figure 6 - Stress-strain results for the characteristic node *P*
(a) stress-strain diagram for the top layer (b) cross-section through the shell

Figure 6(a) contains a characteristic stress-strain curve for the node P of the top surface of the shell marked in Fig. 5(a). The live load was initially increased to an overall of 210 kN (point A in Fig. 6(a)). This load level exceeds the elastic limit for the structure which was found at a total live load of 150 kN. Subsequently, the load level was reduced to 100 kN (point B) and once again increased to a maximum total load of 225 kN (point C). Finally, the live load was removed totally (point D).

The considered point P is characterized by inelastic deformations which correspond to crushing perpendicular to grain, as it is identified by Fig. 6(b). This figure shows the variation of the stress component σ_R over the shell thickness.

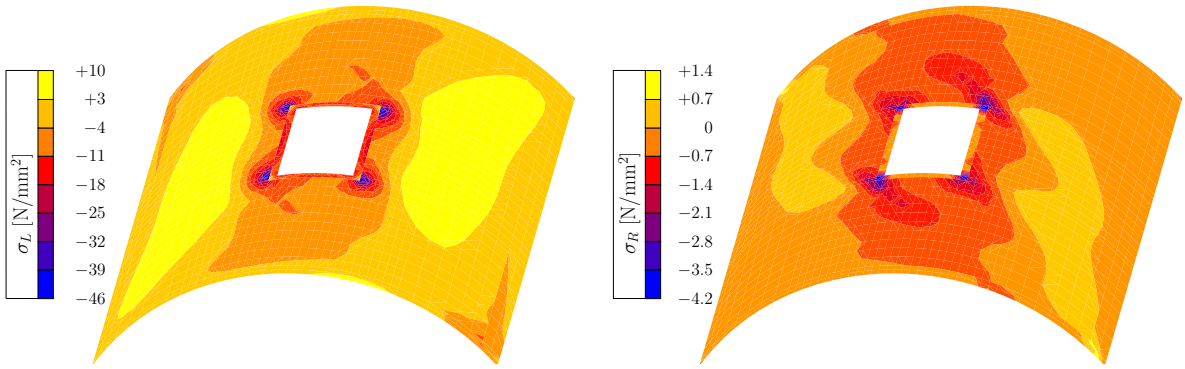

(a) (b)

Figure 7 - Distribution of stress components
(a) fibre stress σ_L in the top layer, (b) radial stress σ_R in the top layer

The shell is subject to both membrane and bending stresses. The latter is dominant near the opening and causes extreme stress values to appear near the corners of the opening. This fact is shown in Fig. 7(a) for the fibre stress σ_L in the top layer of the shell and in Fig. 7(b) for the radial stress σ_R in the top layer of the shell again.

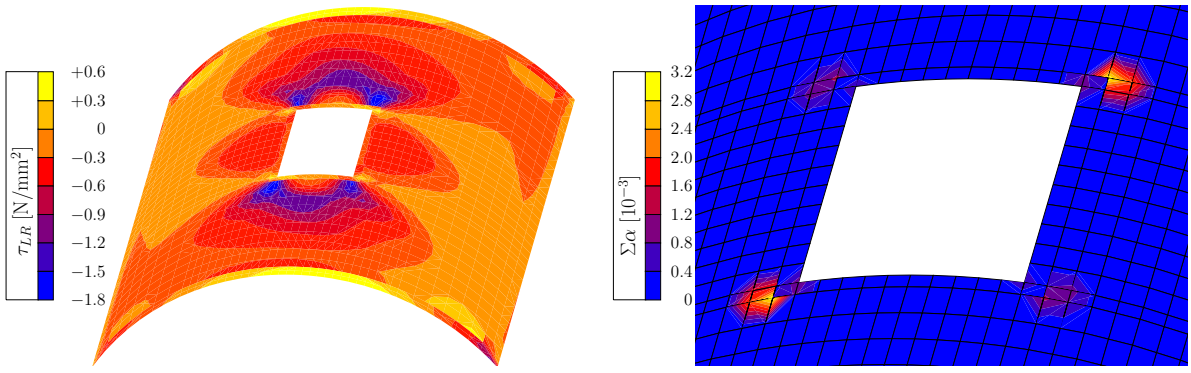

(a) (b)

Figure 8 - Distribution of stress and state variables
(a) in-plane shear stress τ_{LR} in the middle layer, (b) sum of primary variables α_i in the top layer

Figure 8(a) shows the distribution of the in-plane shear stress τ_{LR}. The distribution of the transverse shear stresses τ_{RT} can be found in [5]. Figure 8(b) contains a detail view of the areas with plastic deformations in the top layer of the shell. The picture shows that inelastic deformations only appear in the proximity of the opening. The majority of the shell though remains elastic.

The presented analysis demonstrates that the load bearing capacity of the considered cylindrical shell is controlled by tolerable deformations than by collapse due to material failure. The proposed model, however, can be used to identify critical zones where structural modifications can aid both performance and durability of the wooden shell by reducing local damage.

6. CONCLUSIONS

This paper includes an overview on the development of a new constitutive model for the simulation of clear spruce wood under simultaneous biaxial in-plane stresses and transverse shear stresses. The applicability of the model was proven by means of a nonlinear finite element analysis of a layered cylindrical shell with an opening and surrounding stiffening beams.

The advantages of the proposed formulation are:

- The ability to identify five distinct modes of failure in the material. These modes may be activated individually or as combined failure modes.
- The ability to describe hardening and softening by means of seven distinct strength functions. These functions can be experimentally verified and, if needed, easily replaced by almost any characteristic strength function.
- Due to the single-surface description, the effort for the numerical integration of the rate equations by means of the return mapping algorithm remains moderate.
- A closed form expression for a non-symmetric material tangent operator is available. This is important for an effective numerical implementation.

A verification of the presented material model for plane stress states by means of back-calculations of the biaxial experiments by EBERHARDSTEINER [2] was done by MÜLLNER [6]. The performed simulations of the mentioned experiments show a good agreement between the model and the test results for most modes of biaxial loading. Minor deviations are a consequence of restricting the yield condition to an elliptical surface. However, the obtained results in [6] are superior to any method suggested by design codes.

The presented numerical example gave a brief demonstration of the suitability of the presented material model and its numerical implementation. Further numerical studies with experimental verification on model shells are planned for the near future. In addition to that, the effect of knots and the respective fibre deviations on various strength values is investigated by FLEISCHMANN et al. [3].

References

1. Adalian, C. and Morlier, P. (2002): “Wood Model” for the Dynamic Behaviour of Wood in Multiaxial Compression. Holz als Roh- und Werkstoff, 60 (6): 433-439.
2. Eberhardsteiner, J. (2002): Mechanisches Verhalten von Fichtenholz - Experimentelle Bestimmung der biaxialen Festigkeitseigenschaften. Springer, in German.
3. Fleischmann, M., Eberhardsteiner, J. and Ondris, L. (2003): Experimental Investigation of Spruce Wood in Different Material Directions and Constitutive Modelling Including Knot Effects. 20th Danubia-Adria Symposium on Experimental Methods in Solid Mechanics – Abstracts: 14-15.
4. Mackenzie-Helnwein, P., Eberhardsteiner, J. and Mang, H.A. (2003): A Multi-Surface Plasticity Model for Clear Wood and its Application to the Finite Element Analysis of Structural Details. Computational Mechanics, 31 (1-2): 204-218.
5. Mackenzie-Helnwein, P., Müllner, H.W., Eberhardsteiner, J. and Mang, H.A. (2004): Analysis of Layered Wooden Shells using an Orthotropic Elasto-Plastic Model for Multiaxial Loading of Clear Spruce Wood. Computer Methods in Applied Mechanics and Engineering, in print.
6. Müllner, H.W. (2003): Konstitutives Modellieren von Fichtenholz unter biaxialer Beanspruchung mittels eines orthotropen Einflächenmodells unter Berücksichtigung von Ver- und Entfestigung. Master's Thesis, Vienna University of Technology, in German.
7. Simo, J.C. and Hughes, T.J.R. (1998): Computational Inelasticity – Interdisciplinary Applied Mathematics, Springer.
8. Tsai, S.M. and Wu, E.M. (1971): A General Theory of Strength for Anisotropic Materials. Journal of Composite Materials, 5: 58-80.